C_{60} on SiC Nanomesh

Wei Chen,*,† Hong Liang Zhang,‡ Hai Xu,‡ Eng Soon Tok,‡ Kian Ping Loh,§ and Andrew Thye Shen Wee*,‡

Nanoscience and Nanotechnology Initiative and Department of Physics, National University of Singapore, 2 Science Drive 3, 117542, Singapore, and Department of Chemistry, National University of Singapore, 3 Science Drive 3, 117543, Singapore

Received: July 5, 2006; In Final Form: September 3, 2006

A SiC nanomesh is used as a nanotemplate to direct the epitaxy of C_{60} molecules. The epitaxial growth of C_{60} molecules on SiC nanomesh at room temperature is investigated by in situ scanning tunneling microscopy, revealing a typical Stranski−Krastanov mode (i.e., for the first one or two monolayers, it is a layer-by-layer growth or 2-D nucleation mode; at higher thicknesses, it changes to island growth or a 3-D nucleation mode). At submonolayer (0.04 and 0.2 ML) coverage, C_{60} molecules tend to aggregate to form single-layer C_{60} islands that mainly decorate terrace edges, leaving the uncovered SiC nanomesh almost free of C_{60} molecules. At 1 ML C_{60} coverage, a complete wetting layer of hexagonally close-packed C_{60} molecules forms on top of the SiC nanomesh. At higher coverage from 4.5 ML onward, the C_{60} stacking adopts a (111) oriented face-centered-cubic (fcc) structure. Strong bright and dim molecular contrasts have been observed on the first layer of C_{60} molecules, which are proposed to originate from electronic effects in a single-layer C_{60} island or the different coupling of C_{60} molecules to SiC nanomesh. These STM molecular contrast patterns completely disappear on the second and all the subsequent C_{60} layers. It is also found that the nanomesh can be fully recovered by annealing the C_{60}/SiC nanomesh sample at 200 °C for 20 min.

Introduction

Surface nanotemplates that are artificially or naturally patterned are frequently used to control the self-assembly or self-organization processes on surfaces for the fabrication of two-dimensional (2-D) functional nanostructure arrays with controlled size, shape, and other novel properties such as catalytic, electronic, magnetic, optical, and mechanical properties.[1−20] These surface nanotemplates may have preferential adsorption sites that accommodate individual guest molecules, adatoms, or nanoclusters, favoring the formation of well-ordered nanometer-sized functional arrays.[1,10,13,14,17,18] Recently, intensive research efforts have focused on the fabrication of various surface nanotempletes, as well as the study of the growth behaviors of guest adsorbates (molecules and atoms) on these host nanotemplates, for example, C_{60} molecules on a two-dimensional (2-D) porphyrin-based porous network,[21] C_{60} molecules on boron nitride nanomesh,[18] lander molecules on a O−Cu template,[11] C_{60} molecules on a supramolecular network stabilized by hydrogen bonds,[17] metal atoms on strain-relief patterns,[10] magic clusters on a Si(111)-7 × 7 reconstructured surface,[13−15] and so on. The formation of 2-D nanostructure arrays largely depends on the balance between adsorbate−adsorbate and adsorbate−surface (nanotemplate) interactions.[1] Strong adsorbate−surface interactions at selective adsorption sites on the nanotemplates are desired for the creation of well-ordered nanostructure arrays. The diffusion of adsorbed molecules, atoms, and clusters on the nanotemplate surfaces also plays an essential role during the formation of 2-D nanostructure arrays.[10] Hence, detailed investigations of the nucleation and growth of adsorbates (molecules, atoms, or clusters) on the surface nanotemplates are needed to better understand and control the formation of well-ordered 2-D nanostructure arrays.

We have previously used the SiC nanomesh template on 6H−SiC(0001) for the growth of size-controlled metal clusters.[22,23] This SiC nanomesh arises from the self-organization of excess carbon atoms forming a honeycomb arrangement on 6H−SiC-(0001) after annealing at 1100 °C.[24] In this paper, we expand the use of the SiC nanomesh template to direct the epitaxy of C_{60} molecules. The detailed growth behaviors are systematically investigated by in situ scanning tunneling microscopy, revealing a typical Stranski−Krastanov mode (i.e., for the first one or two C_{60} monolayers, it is a layer-by-layer growth or 2-D nucleation mode; at higher thickness, it changes to island growth or a 3-D nucleation mode). A complete wetting layer of hexagonally close-packed C_{60} molecules forms on top of the SiC nanomesh at 1 ML coverage. Annealing the C_{60}/SiC nanomesh at 200 °C for 20 min leads to the thorough desorption of C_{60} molecules and the regeneration of the underlying SiC nanomesh,

Experimental Procedures

The STM experiments were conducted with a commercial variable temperature scanning tunneling microscope (Omicron VT-STM) housed in a multi-chamber UHV system with a base pressure of 1.0×10^{-10} Torr.[25] A *n*-type Si-terminated 6H−SiC(0001) sample (CREE Research Inc.) was chemically etched in 10% HF solution for 1.5 min, followed by 3 min of ultrasonic

* Corresponding authors. E-mail: (W.C.) nnicw@nus.edu.sg and (A.T.S.W.) phyweets@nus.edu.sg.
† Nanoscience and Nanotechnology Initiative.
‡ Department of Physics.
§ Department of Chemistry.

10.1021/jp0642241 CCC: $33.50
Published on Web 09/29/2006

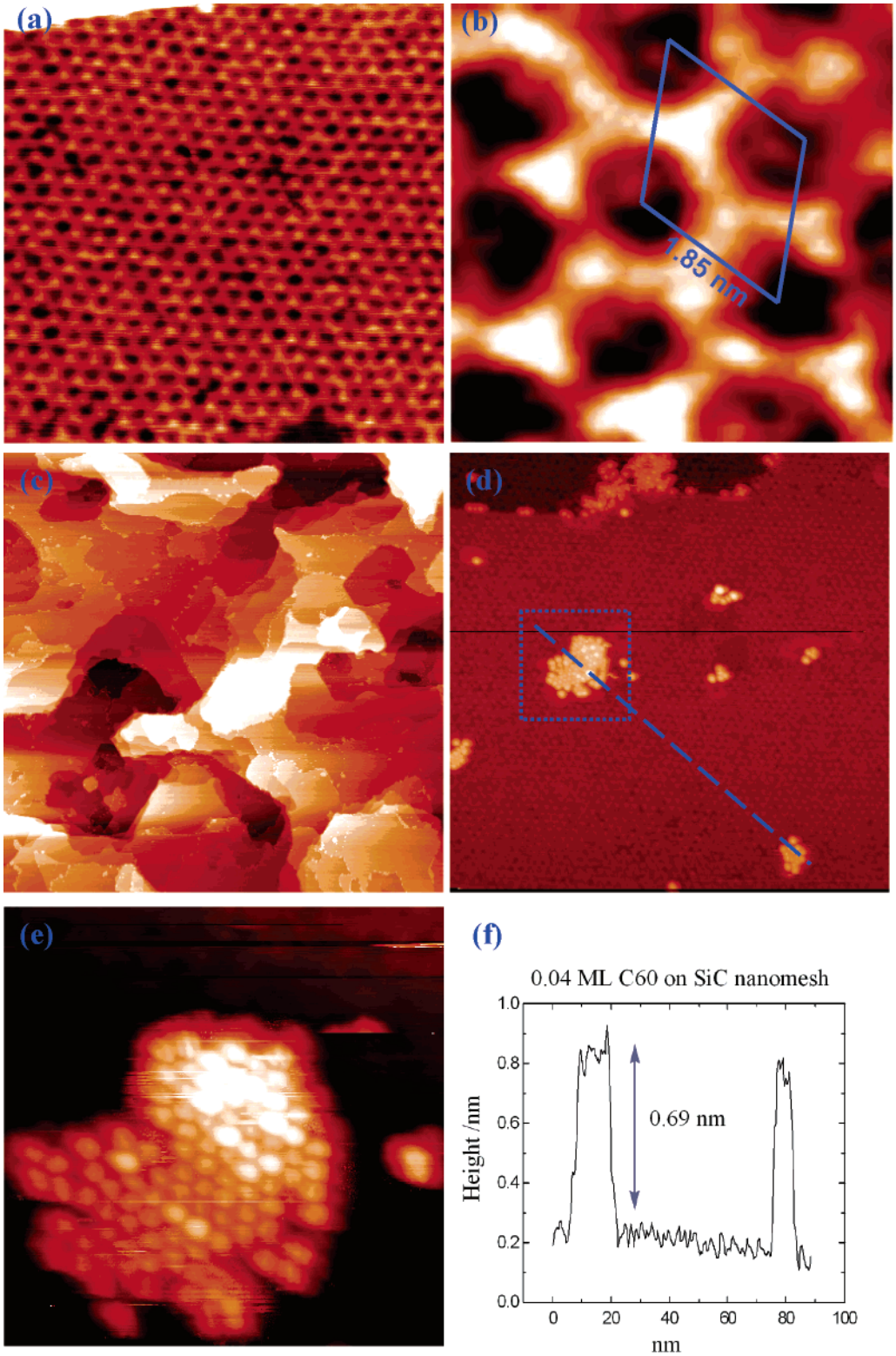

Figure 1. STM images of SiC nanomesh clean surface: (a) 40 nm × 40 nm and (b) detailed 5.5 nm × 5.5 nm image showing the 6 × 6 unit cell. Covered with 0.04 ML C60: (c) 1000 nm × 1000 nm, (d) 80 nm × 80 nm, and (e) corresponding detailed 20 nm × 20 nm image as highlighted by dashed squares in panel d. (f) Line profile as marked by the dashed line in panel d. $I_{tunneling} = 130$ pA and $V_{sample} = -1.8$ V for panels a and b and $I_{tunneling} = 50$ pA and $V_{sample} = -1.2$ V for panels c−e.

rinsing in deionized water. After etching, the SiC sample was immediately transferred into the UHV chamber and degassed at 500 °C overnight. The sample was then annealed at 850 °C under a silicon flux for 2 min, resulting in a Si-rich 3 × 3 reconstructed surface,[25−27] and subsequently annealed several times at 1100 °C in the absence of the silicon flux to form the carbon-rich nanomesh surface.[22−24,28] C_{60} molecules (Sigma-Aldrich, 99.9%) were evaporated in situ from a low-temperature Knudsen cell onto SiC nanomesh substrates at room temperature in the main UHV chamber. Before deposition, the C_{60} was thoroughly degassed at 250 °C in UHV condition. The deposition of C_{60} was performed at a constant rate of about 0.02 ML/min. Since the first C_{60} layer growth mode is almost layer-by-layer, the deposition rate was calibrated using large-scale STM

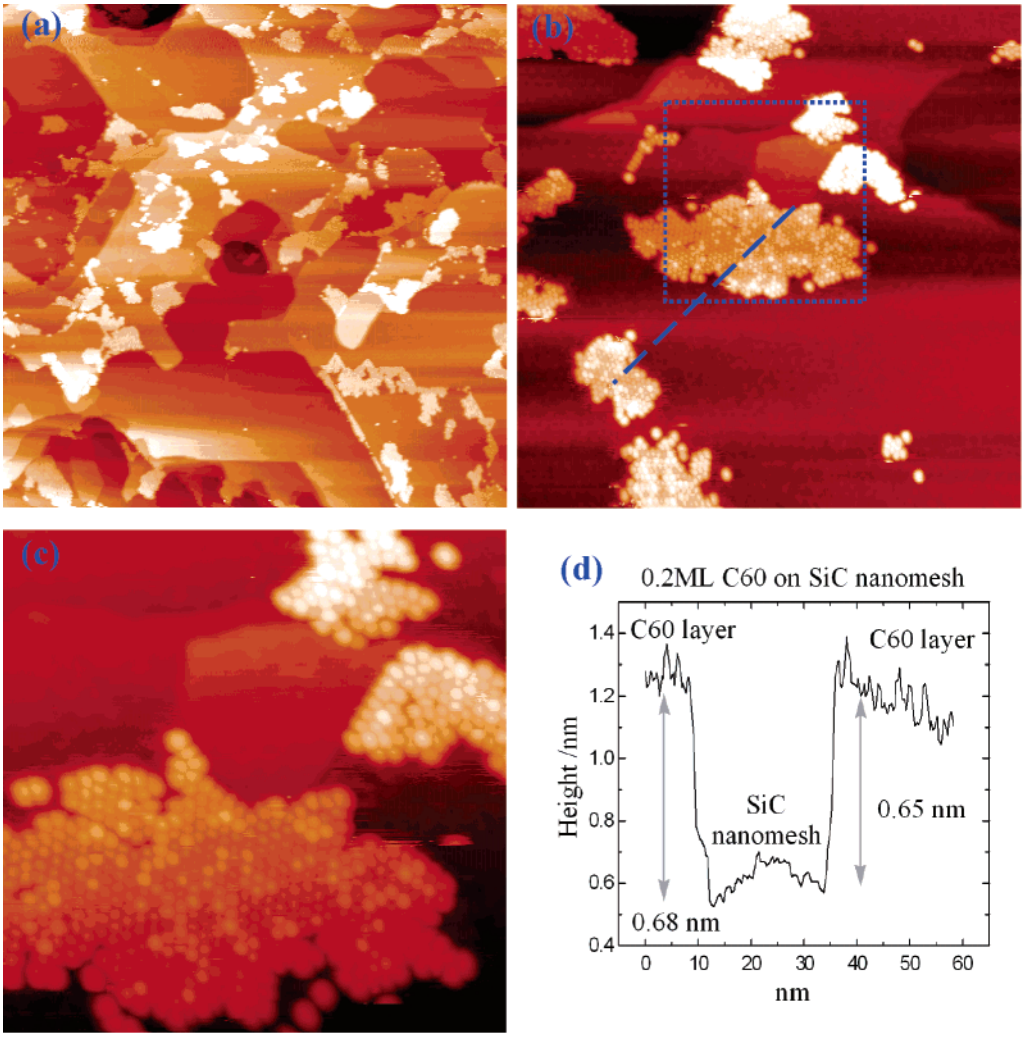

Figure 2. STM images of 0.2 ML C_{60} on SiC nanomesh surface: (a) 500 nm × 500 nm, (b) 100 nm × 100 nm, (c) corresponding detailed 40 nm × 40 nm image of C_{60} single-layer island as highlighted by dashed squares in panel b, and (d) the line profile as marked by the dashed line in panel b. $I_{tunneling} = 30$ pA and $V_{sample} = +1.4$ V.

images with coverage below 1 ML (1 ML = one layer of fully covered C_{60}). During deposition, the chamber pressure was maintained below 4.0×10^{-10} Torr.

Results and Discussion

Growth Behaviors of C_{60} on SiC Nanomesh. Figure 1a shows the typical STM filled state image of SiC nanomesh formed after annealing 6H−SiC(0001) at 1100 °C. This SiC nanomesh comprises incommensurate honeycombs with a periodicity close to 6 × 6, which arises from the self-organization of excess carbon atoms at elevated temperature accompanied by the evaporation of Si atoms from SiC surface.[24] The detailed structure of this surface is displayed in Figure 1b, which clearly shows the unit cell of the nanomesh superstructure. C_{60} molecules were evaporated onto this nanomesh at room temperature to evaluate the effectiveness of this nanomesh for the growth of well-ordered 2-D nanostructures. At the low coverage of 0.04 ML, C_{60} molecules mainly decorated substrate terrace edges as shown by the large-scale 1000 nm × 1000 nm STM image in Figure 1c. Very few C_{60} tiny islands were found to nucleate on the SiC nanomesh terraces (Figure 1d). The corresponding line profile (Figure 1(f) of these islands shows that the island height is about 0.69 ± 0.02 nm. As such, these tiny islands can be interpreted as single-layer C_{60} islands.[29,30] The molecular-resolved STM image in Figure 1e displays the C_{60} arrangement in the single-layer island, revealing a hexagonally close-packed structure. Figure 2a shows the 500 nm × 500 nm STM empty state image of 0.2 ML C_{60} on SiC nanomesh. Similar to the 0.04 ML coverage, the C_{60} molecules tent to aggregate to form separate C_{60} islands as shown in Figure 2b, leaving the uncovered regions of SiC nanomesh unchanged. The C_{60} island had a irregular shape as shown in Figure 2b. The line profile of the C_{60} island (Figure 2d) clearly reveals that the island is a single-layer high. The C_{60} molecular arrangement kept the hexagonally close-packed structure as displayed by the molecular-resolved STM image in Figure 2c. We have previously investigated the detailed growth behaviors of Co nanoclusters on this SiC nanomesh.[22,23] It is found that Co nanoclusters preferred to adsorb on the corner sites of SiC nanomesh at the initial growth stage,[22] suggesting the relatively strong interaction between Co nanoclusters and SiC nanomesh. However, we did not observe any preferential C_{60} adsorption sites on SiC nanomesh. The aggregation behavior of C_{60} molecules on SiC nanomesh observed here indicates that the interaction strength of the SiC nanomesh with C_{60} is weaker than that with Co nanoclusters, favoring the formation of hexagonally close-packed C_{60} single-layer islands.

Increasing the coverage to 0.5 ML led to the coalescence of small C_{60} molecular islands to form bigger islands, as shown in the 1000 nm × 1000 nm image of Figure 3a and the 200 nm

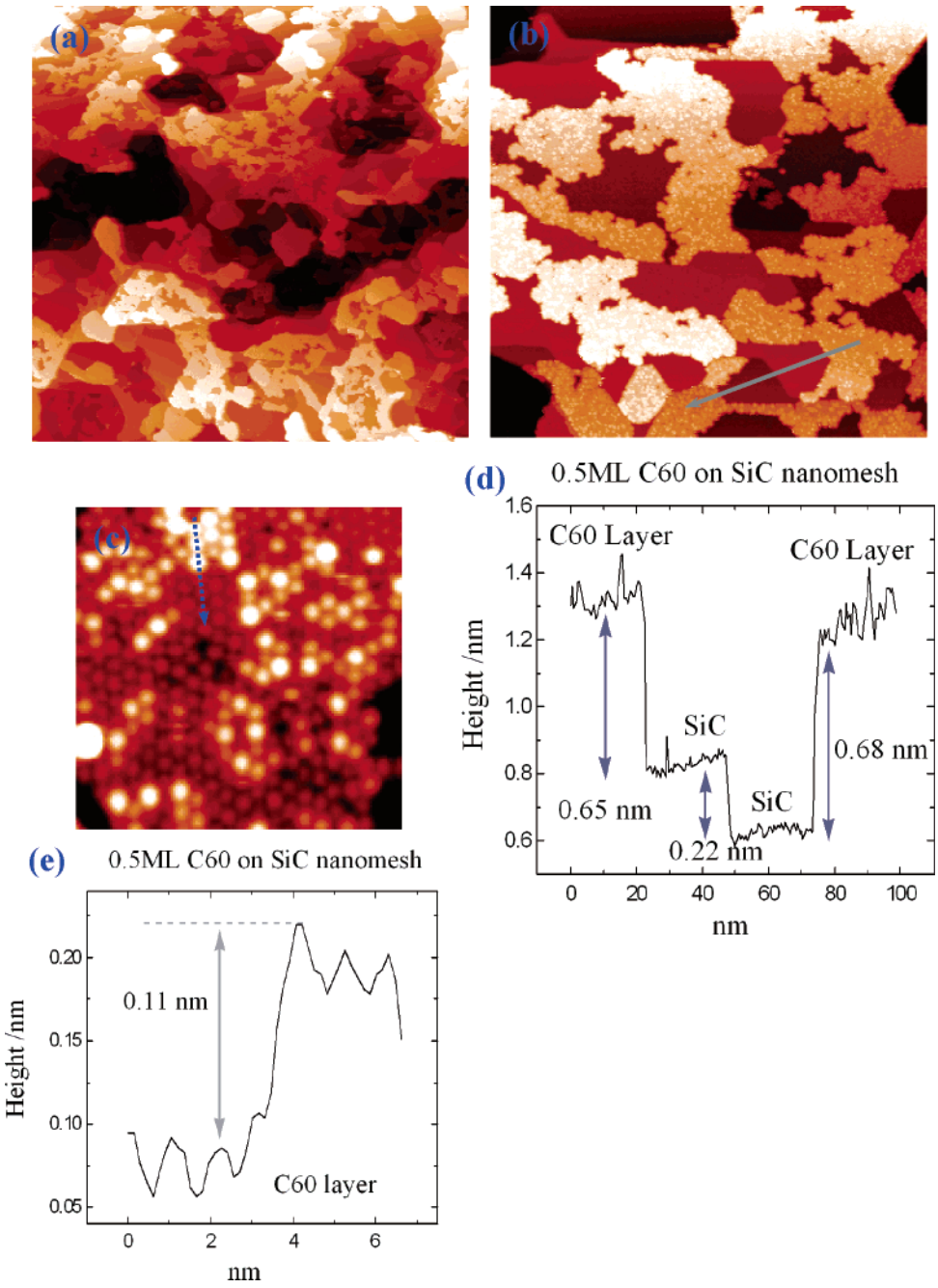

Figure 3. STM empty state images of 0.5 ML C_{60} on SiC nanomesh surface: (a) 1000 nm × 1000 nm, (b) detailed 200 nm × 200 nm, and (c) 20 nm × 20 nm images. (d) Line profile as highlighted by the arrow in panel b and (e) line profile as marked by the dashed arrow in panel c. $I_{tunneling} = 35$ pA and $V_{sample} = +1.4$ V.

× 200 nm image in Figure 3b. Figure 3d shows the line profile of a C_{60} island beside a substrate terrace edge, marked by the arrow in Figure 3b. It clearly reveals that the C_{60} island is one molecular layer high. On top of these C_{60} single-layer islands, no second C_{60} layer was found in all areas imaged, suggesting that the first-layer growth of C_{60} on the SiC nanomesh is a layer-by-layer growth mode. Figure 3c is a 20 nm × 20 nm image of a C_{60} island showing random variation in C_{60} image contrast. The line profile (Figure 3e) reveals that the height difference between the bright and the dim C_{60} molecules is around 0.11 ± 0.02 nm, much smaller than the diameter of a C_{60} molecule. As such, the bright domains are not due to second-layer C_{60} molecules; they must be interpreted as undulations or electronic effects in a single-layer C_{60} island. Liu et al. have reported the initial growth stage of C_{60} thin films on a graphite substrate.[31] The first layer of C_{60} forms spherical, monolayer high islands; the second and all subsequent layers adopt a highly branched fractal−dendritic shape. It was suggested that the profound difference in the first- and second-layer growth originates from the significant difference in the diffusion energy barriers of C_{60} molecules on graphite and C_{60} thin film surfaces according to a diffusion-limited aggregation. As shown in Figure 2(b) and Figure 3(b), the first-layer C_{60} islands on SiC nanomesh adopt an irregular shape, and not the spherical shape nor the fractal-dendritic shape. Since SiC nanomesh can be described as a surface with periodic corrugation, C_{60} molecules are expected to experience a higher diffusion barrier than on flat graphite surface. The formation of irregularly shaped C_{60} first-layer can, therefore, be attributed to the constrained diffusion of C_{60} molecules on SiC nanomesh at room temperature.

The complete wetting layer of C_{60} molecules on SiC nanomesh was achieved by increasing the coverage to 1 ML.

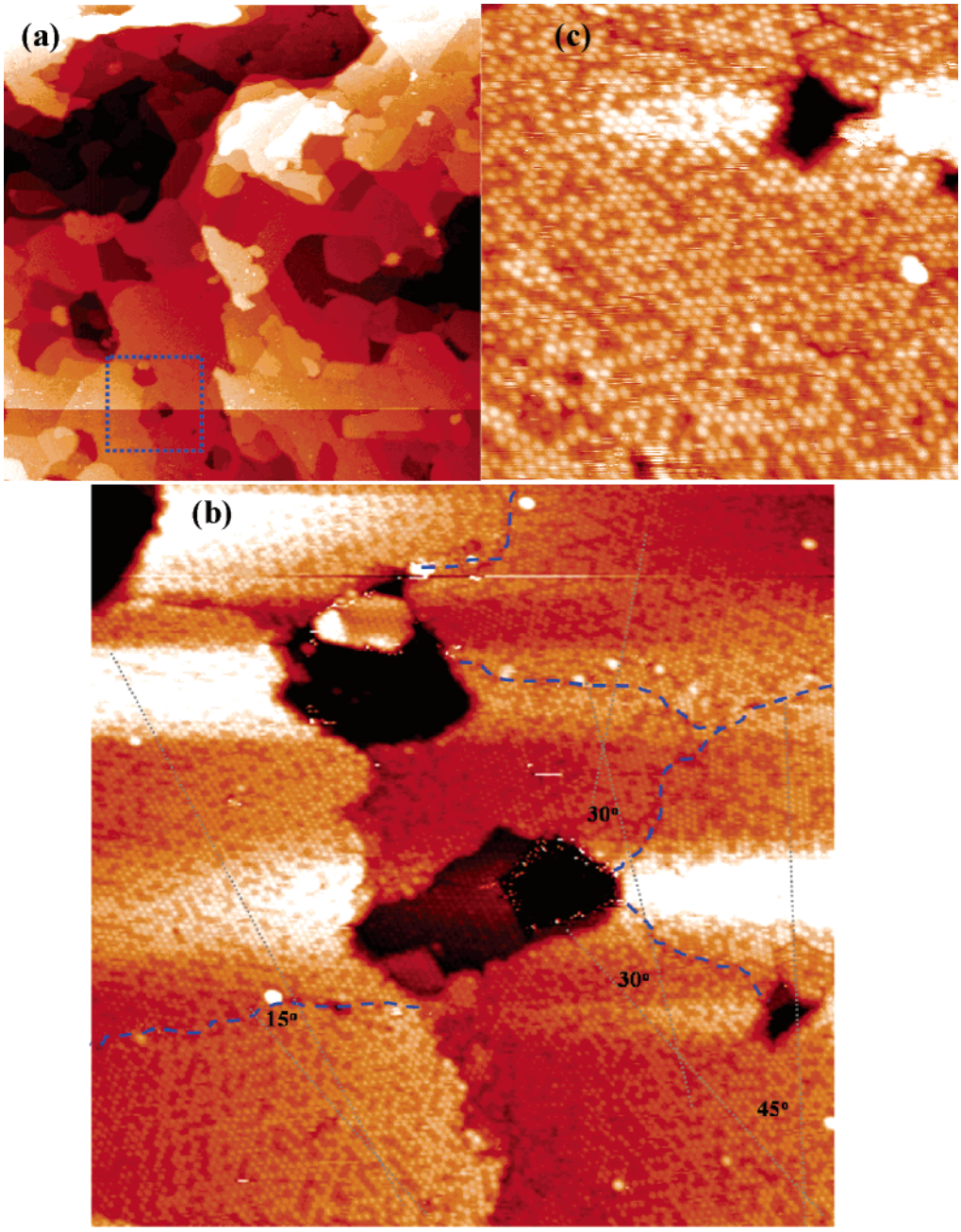

Figure 4. STM empty state images of 1 ML C_{60} on SiC nanomesh surface: (a) 500 nm × 500 nm, (b) detailed 100 nm × 100 nm image as marked by dashed squares in panel a, and (c) 40 nm × 40 nm. $I_{tunneling} = 45$ pA and $V_{sample} = +1.4$ V.

As shown in Figure 4(a), SiC nanomesh was fully covered by a C_{60} monolayer, with a few small C_{60} islands on top, confirming that the first-layer growth mode is layer-by-layer. The molecular-resolved STM image (Figure 4b) shows the well-packed C_{60} monolayer structure. Domains of the C_{60} monolayer on SiC nanomesh with different rotations were observed, and the rotation angles were highlighted in Figure 4b. The dashed lines indicate the domain boundaries. As shown in Figure 4b, the surface morphology exhibits a two-level bright−dim C_{60} contrast pattern. This contrast pattern can be seen more clearly in the 40 nm × 40 nm empty state image in Figure 4c. The line profile (not shown here) reveals a small height difference (~0.07 ± 0.02 nm) between the bright and the dim C_{60} molecules, confirming that all the C_{60} molecules are in the same molecular layer.

By increasing the C_{60} coverage to 1.4 ML, small irregularly shaped single-layer C_{60} islands formed on top of the first C_{60} layer as shown in the 1000 nm × 1000 nm image in Figure 5a. Third-layer C_{60} formation on these irregular C_{60} islands was rarely found by careful analysis of many images, indicating that the second layer still follows the layer-by-layer growth mode. Figure 5b shows a molecular-resolved STM image revealing a hexagonally close-packed second C_{60} layer. Figure 5c displays the 1000 nm × 1000 nm image of 3 ML C_{60} on SiC nanomesh. A large number of irregularly shaped C_{60} islands nucleated on top of the underlying incomplete C_{60} layers, suggesting that the growth of C_{60} is transiting to the island growth mode. The C_{60} molecular arrangement on the top layer kept a hexagonally close-packed structure, as shown in Figure 5d. The previously observed bright−dim contrast patterns on the first C_{60} layer (Figures 3c and 4c) cannot be seen on the top C_{60} layer at this stage.

The characteristic island growth behavior of C_{60} on SiC nanomesh can be observed more clearly at higher coverage.

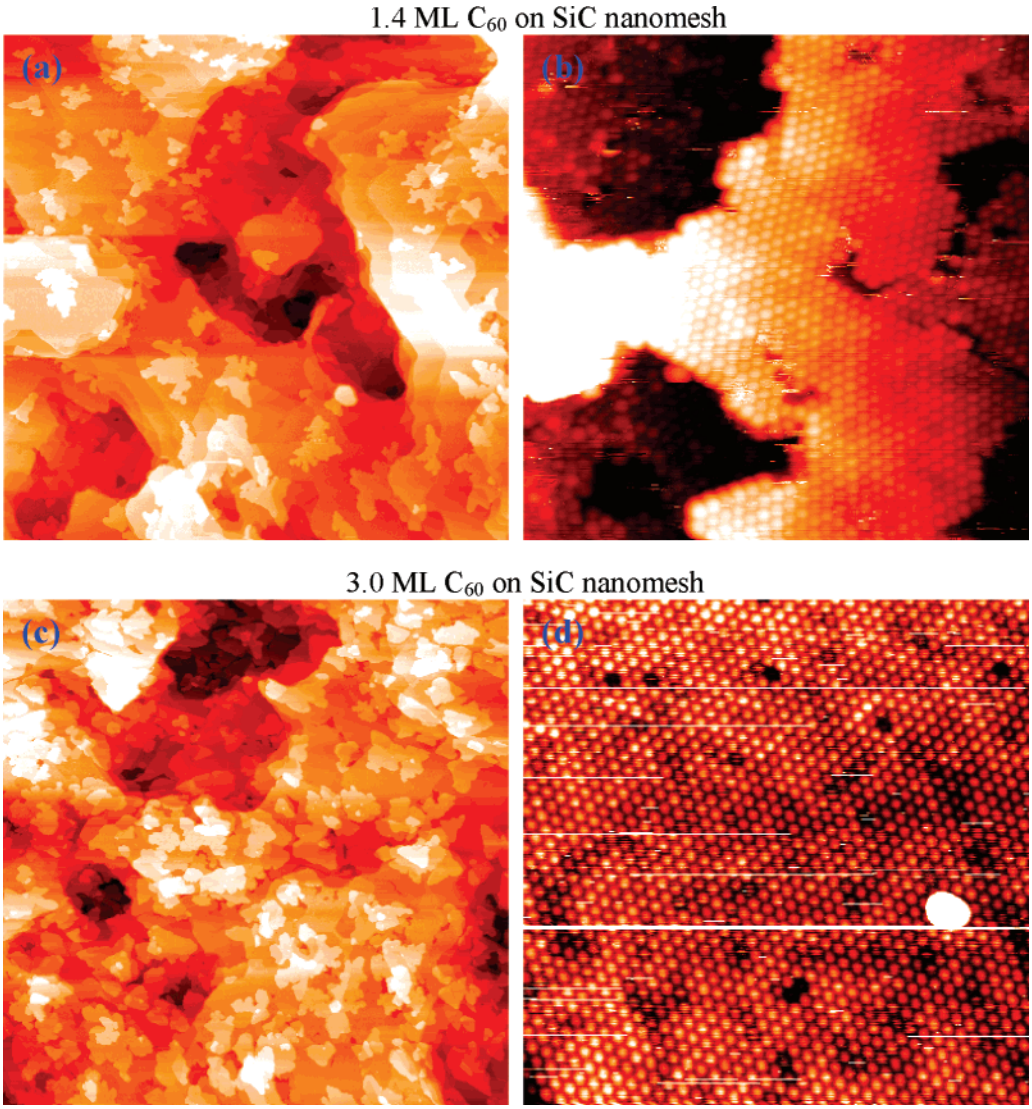

Figure 5. 1000 nm × 1000 nm STM empty state images of SiC nanomesh surfaces with (a) 1.4 ML, (c) 3 ML C_{60}, and corresponding detailed images: (b) 40 nm × 40 nm and (d) 60 nm × 60 nm, respectively. $I_{tunneling} = 65$ pA and $V_{sample} = +1.4$ V for panels a and b and $I_{tunneling} = 115$ pA and $V_{sample} = +1.4$ V for panels c and d.

Figure 6a shows a 500 nm × 500 nm STM image of 4.5 ML C_{60} on SiC nanomesh, where stacked irregularly shaped C_{60} islands nucleated on top of underlying C_{60} layers. The size of the islands is around a few hundred nanometers. The result reveals that the growth of C_{60} on the SiC nanomesh at higher coverage has transformed to island growth or 3-D nucleation mode. Therefore, the growth of C_{60} on SiC nanomesh can be described as a typical Stranski−Krastanov growth mode.[32] Figure 6b is an 80 nm × 80 nm STM empty state image showing the defect-free hexagonally close-packed C_{60} molecules on each terrace. The C_{60} molecular arrangement on the top C_{60} layer is shown by a high-resolution STM empty state image in Figure 6c. The line profile (not shown here) of C_{60} molecules on the top layer reveals that the C_{60} intermolecular distance (0.99 ± 0.02 nm) is very close to the nearest-neighboring distance (1.00 nm) reported in the literature,[30,33−35] suggesting that the C_{60} stacking adopts a (111) oriented face-centered-cubic (fcc) structure. At 7.5 ML, the growth of C_{60} on SiC nanomesh continued in the island growth mode. As shown in Figure 6d,e, more C_{60} islands were stacked on the surface. C_{60} molecular arrangement on the stacked islands is shown in the molecular-resolved STM image in Figure 6f, clearly showing that the hexagonally close-packed structure observed in Figure 6c is retained.

The original SiC nanomesh can be fully regenerated by annealing the 6 ML C_{60}/nanomesh sample at 200 °C for 20 min. STM images of the regenerated SiC nanomesh are almost identical to the original nanomesh (Figure 1a,b). This clearly demonstrates that the adsorption of C_{60} molecules does not change the nanomesh structure. We have previously observed a similar regeneration of SiC nanomesh with a full adlayer of Co nanoclusters.[22,23] SiC nanomesh is easily regenerated by the complete desorption of Co nanoclusters at much higher temperatures of around 1100°C, indicating the good thermal stability and chemical inertness of SiC nanomesh to adsorbed molecules and atoms.[22,23] It was reported that the complete desorption of C_{60} from the HOPG surface takes place between 510 and 530 K[36] (i.e., 237−257 °C), close to the desorption temperature of C_{60} molecules from SiC nanomesh This indicates that the interaction strength between the two surfaces (HOPG and SiC nanomesh) and the C_{60} molecules cannot be very different. Hence, the interaction between C_{60} molecules and SiC nanomesh is expected to be dominated by van der Waals forces.

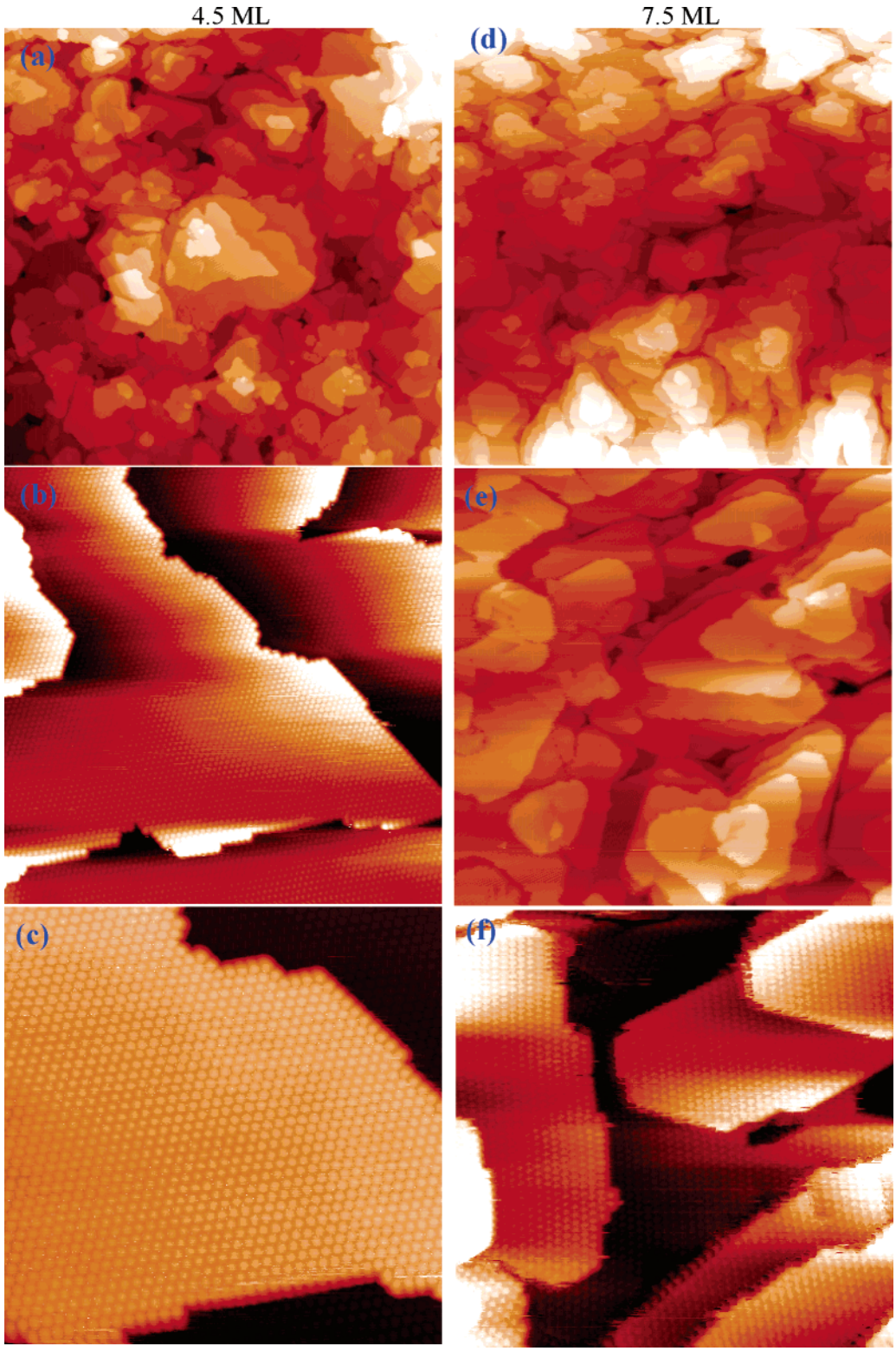

Figure 6. STM empty state images of 4.5 ML (a−c) and 7.5 ML (d−f) C_{60} on SiC nanomesh surface: (a and d) 500 nm × 500 nm, (b) 80 nm × 80 nm, (c) 40 nm × 40 nm, (e) 200 nm × 200 nm, and (f) 50 nm × 50 nm. $I_{tunneling}$ = 0.5 nA and V_{sample} = +1.3 V for panels a−c and $I_{tunneling}$ = 1.5 nA and V_{sample} = +1.3 V for panels d−f.

Bright−Dim Molecular Contrast Pattern of C_{60} on SiC Nanomesh. Bright−dim STM molecular contrast patterns were observed for the submonolayer and monolayer of C_{60} on SiC nanomesh. For example, the surface exhibited a two-level bright−dim C_{60} contrast pattern (type A) for 1 ML C_{60} coverage as shown in Figure 4c. Figure 7a shows the STM empty state image on another area of the same 1ML C_{60}/SiC nanomesh. Besides the type A bright−dim contrast pattern that was similar to Figure 4c, a more disordered bright−dim contrast pattern (type B) was also found on the same area. The arrows in Figure 7a highlight the type A and B contrast patterns in the same surface. The line profile (Figure 7c) clearly reveals that both types of contrast patterns (type A and B) are located in the same C_{60} molecular layer. Figure 7b shows the detailed 20 nm × 20 nm STM image in the type A contrast pattern in Figure 7a, where the dim C_{60} molecules are visible. The line profile (Figure

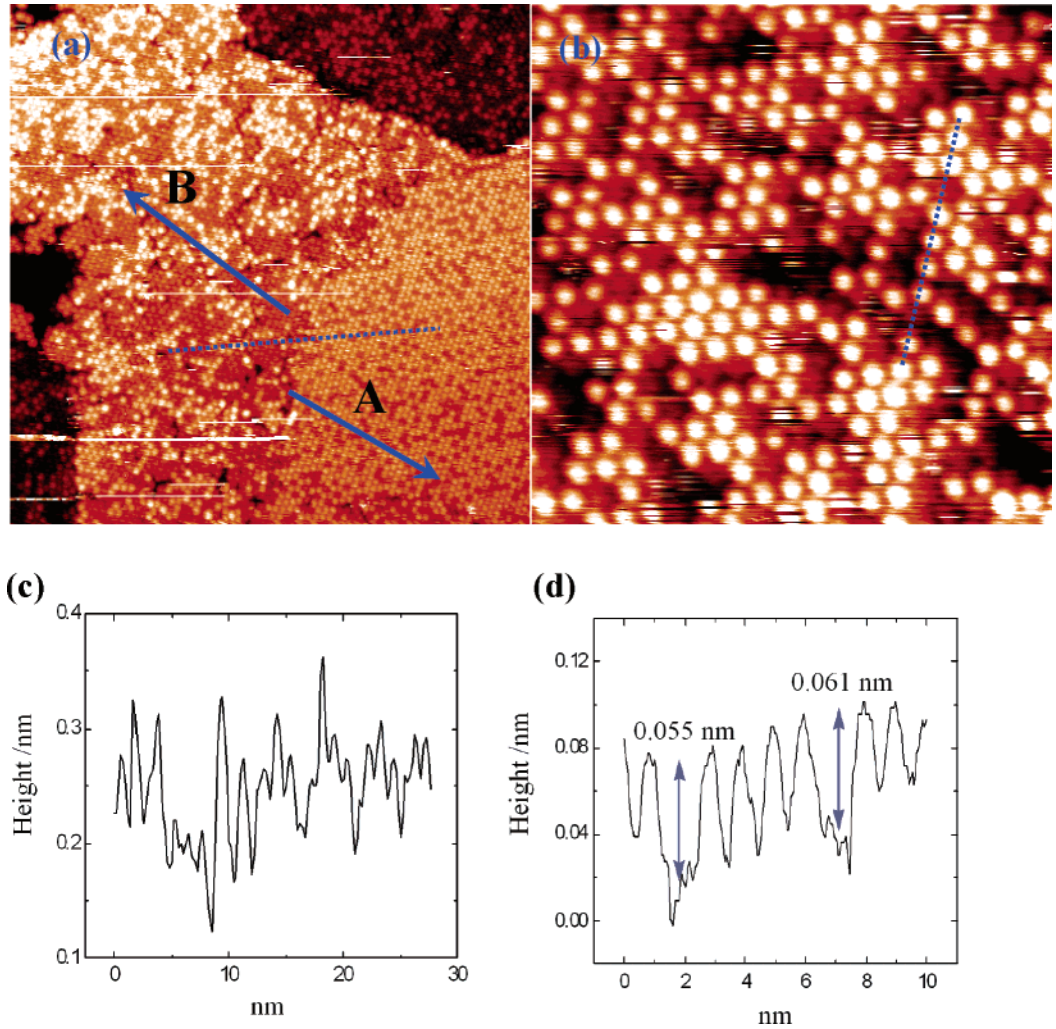

Figure 7. STM empty state images of 1 ML C_{60} on SiC nanomesh surface in another area: (a) 80 nm × 80 nm image and corresponding detailed (b) 20 nm × 20 nm images in type A contrast patterns as shown in panel a. Panels c and d show the line profiles as marked by dashed lines in panels a and b, respectively. $V_{sample} = +1.0$ V.

7d) shows that the height difference between the bright and the dim C_{60} molecules is only around 0.05−0.06 nm. For submonolayer C_{60} on SiC nanomesh (Figure 3e), this height difference can be as much as 0.11 nm in some cases. A previous study reveals that two different orientations of a C_{60} molecule (i.e., with a hexagonal ring and a pentagonal ring in contact with substrate surface, respectively) induce a geometrical height difference of around 0.02 nm.[37] This height difference is much smaller than that between the bright and the dim C_{60} molecules observed on the type A and B contrast patterns of 1 ML C_{60} on SiC nanomesh, indicating that the bright−dim contrast patterns in Figures 4 and 7 did not originate from the different orientations of the C_{60} molecules.

Similar bright−dim STM contrast patterns of C_{60} molecules on metal surfaces have been previous observed, which are due to C_{60}-induced reconstruction underneath the dim C_{60} molecules.[33,38−41] As we previously reported, the SiC nanomesh arises from the self-organization of an excess carbon atoms on the 6H−SiC(0001) surface.[24] As such, the SiC nanomesh surface is almost fully covered by carbon atoms. The height difference between bright and dim C_{60} molecules observed here that varied from 0.05 to 0.11 nm, however, is certainly too small for the height of a single layer of carbon atoms. Therefore, the bright−dim STM contrast patterns (type A and B) are not due to C_{60}-induced reconstruction underneath the dim C_{60} molecules. In our experiment, the bright−dim contrast patterns were found to only occur on the C_{60} layer in direct contact with the underlying SiC nanomesh (i.e., submonolayer or monolayer condition; while for the second and all the subsequent C_{60} layers, the STM contrast patterns vanished as shown in Figures 5 and 6). As such, the bright−dim contrast patterns in the first layer of C_{60} on SiC nanomesh most likely originate from electronic effects in the single-layer C_{60} island or the different coupling of C_{60} molecules to the SiC nanomesh at different sites. Because of the complexity of the SiC nanomesh, the nature of the interaction between the first-layer C_{60} molecules and the SiC nanomesh cannot be thoroughly elucidated by STM study. Future experiments using synchrotron photoelectron spectroscopy will be carried out to address this question.

Conclusion

In situ scanning tunneling microscopy was used to systematically investigate the growth behaviors of C_{60} molecules on SiC nanomesh at room temperature. The growth of C_{60} on SiC nanomesh displays a typical Stranski−Krastanov mode (i.e., the first one or two monolayers form via layer-by-layer growth or 2-D nucleation mode; at higher thickness, it transforms to island growth or a 3-D nucleation mode). After deposition of 1 ML C_{60}, a complete layer of hexagonally close-packed C_{60} molecules forms on top of the SiC nanomesh. The observed bright−dim STM molecular contrast patterns on the first layer of C_{60} in

direct contact with the underlying SiC nanomesh are proposed to originate from electronic effects in a single-layer C_{60} island or the different coupling of C_{60} molecules to SiC nanomesh at different sites. At higher coverage from 4.5 ML onward, the C_{60} stacking adopts a (111) oriented face-centered-cubic (fcc) structure; at the same time, those bright−dim STM molecular contrast patterns completely disappear on the top C_{60} layer. Finally, the nanomesh can be fully recovered by annealing the C_{60}/SiC nanomesh sample at 200 °C for 20 min. Since the nanomesh on the SiC surface is a unique carbon form and closely related to graphene, detailed investigations of the growth of C_{60} and other molecules on SiC nanomesh would be of fundamental interest. Furthermore, the formation of well-packed C_{60} thin films on SiC substrates may have future applications in the field of molecular field-effect transistors and organic solar cells, where SiC nanomesh could serve as templates for the growth of well-ordered organic films.

Acknowledgment. W.C. acknowledges the support from the A*STAR Grant R-398-000-036-305.

References and Notes

(1) Rosei, F. *J. Phys.: Condens. Matter* **2004**, *16*, S1373.
(2) Rosei, F.; Schunack, M.; Jiang, P.; Gourdon, A.; Laegsgaard, E.; Stensgaard, I.; Joachim, C.; Besenbacher, F. *Science* **2002**, *296*, 328.
(3) Barth, J. V.; Weckesser, J.; Cai, C.; Günter, P.; Bürgi, L.; Jeandupeux, O.; Kern, K. *Angew. Chem., Int. Ed.* **2000**, *39*, 1230.
(4) Weckesser, J.; De Vita, A.; Barth, J. V.; Cai, C.; Kern, K. *Phys. Rev. Lett.* **2001**, *87*, 096101.
(5) Spillmann, H.; Dmitriev, A.; Lin, N.; Messina, P.; Barth, J. V.; Kern, K. *J. Am. Chem. Soc.* **2003**, *125*, 10725.
(6) Barth, J. V.; Weckesser, J.; Trimarchi, G.; Vladimirova, M.; De Vita, A.; Cai, C.; Brune, H.; Günter, P.; Kern, K. *J. Am. Chem. Soc.* **2002**, *124*, 7991.
(7) de Feyter, S.; Gesquiére, A.; Klapper, M.; Mullen, K.; DeSchryver, F. C. *Nano Lett.* **2003**, *3*, 1485.
(8) Barth, J. V.; Constantini, G.; Kern, K. *Nature* **2005**, *437*, 671.
(9) Berner, S.; de-Wild, M.; Ramoino, L.; Ivan, S.; Baratoff, A.; Güntherodt, H.-J.; Suzuki, H.; Schlettwein, D.; Jung, T. A. *Phys. Rev. B* **2003**, *68*, 115410.
(10) Brune, H.; Giovannini, M.; Bromann, K.; Kern, K. *Nature* **1998**, *394*, 451−453.
(11) Otero, R.; Naitoh, Y.; Rosei, F.; Jiang, P.; Thostrup, P.; Gourdon, A.; Laegsgaard, E.; Stensgaard, I.; Joachim, C.; Besenbacher, F. *Angew. Chem., Int. Ed.* **2004**, *43*, 2092.
(12) Rosei, F.; Rosei, R. *Surf. Sci.* **2002**, *500*, 395.
(13) Wu, K. H.; Fujikawa, Y.; Nagao, T.; Hasegawa, Y.; Nakayama, K. S.; Xue, Q. K.; Wang, E. G.; Briere, T.; Kumar, V.; Kawazoe, Y.; Zhang, S. B.; Sakurai, T. *Phys. Rev. Lett.* **2003**, *91*, 126101.
(14) Li, J. L.; Jia, J. F.; Liang, X. J.; Liu, X.; Wang, J. Z.; Xue, Q. K.; Li, Z. Q.; Tse, J. S.; Zhang, Z. Y.; Zhang, S. B. *Phys. Rev. Lett.* **2002**, *88*, 066101.
(15) Lai, M. Y.; Wang, Y. L. *Phys. Rev. B* **2001**, *64*, 241404.
(16) Kotlyar, V. G.; Zotov, A. V.; Saranin, A. A.; Kasyanova, T. V.; Cherevik, M. A.; Pisarenko, I. V.; Lifshits, V. G. *Phys. Rev. B* **2002**, *66*, 165401.
(17) Theobald, J. A.; Oxtoby, N. S.; Phillips, M. A.; Champness, N. R.; Beton, P. H. *Nature* **2003**, *424*, 1029.
(18) Corso, M.; Auwärter, W.; Muntwiler, M.; Tamai, A.; Greber, T.; Osterwalder, J. *Science* **2004**, *303*, 217.
(19) Cicoira, F.; Rosei, F. *Surf. Sci.* **2006**, *600*, 1.
(20) Nath, K. G.; Ivasenko, O.; Miwa, J. A.; Dang, H.; Wuest, J. D.; Nanci, A.; Perepichka, D. F.; Rosei, F. *J. Am. Chem. Soc.* **2006**, *128*, 4212.
(21) Spillmann, H.; Kiebele, A.; Stöhr, M.; Jung, T. A.; Bonifazi, D.; Cheng, F.; Diederich, F. *Adv. Mater.* **2006**, *18*, 275.
(22) Chen, W.; Loh, K. P.; Xu, H.; Wee, A. T. S. *Langmuir* **2004**, *20*, 10779.
(23) Chen, W.; Loh, K. P.; Xu, H.; Wee, A. T. S. *Appl. Phys. Lett.* **2004**, *84*, 281.
(24) Chen, W.; Xu, H.; Liu, L.; Gao, X. Y.; Qi, D. C.; Peng, G. W.; Tan, S. C.; Feng, Y. P.; Loh, K. P.; Wee, A. T. S. *Surf. Sci.* **2005**, *596*, 176.
(25) Chen, W.; Xie, X. N.; Xu, H.; Wee, A. T. S.; Loh, K. P. *J. Phys. Chem. B* **2003**, *107*, 11597.
(26) Ong, J.; Tok, E. S.; Xu, H.; Wee, A. T. S. *Appl. Phys. Lett.* **2002**, *80*, 3406.
(27) Chen, W.; Xu, H.; Loh, K. P.; Wee, A. T. S. *Surf. Sci.* **2005**, *595*, 107.
(28) Ong, W. J.; Tok, E. S. *Phys. Rev. B* **2006**, *73*, 045330.
(29) Hou, J. G.; Yang, J. L.; Wang, H. Q.; Li, Q. X.; Zeng, C. G.; Yuan, L. F.; Wang, B.; Chen, D. M.; Zhu, Q. S. *Nature* **2001**, *409*, 304.
(30) Heiney, P. A.; Fischer, J. E.; McGhie, A. R.; Romanow, W. J.; Denenstein, A. M.; McCauley, J. P.; Smith, A. B.; Cox, D. E. *Phys. Rev. Lett.* **1991**, *66*, 2911.
(31) Liu, H.; Reinke, P. *J. Chem. Phys.* **2006**, *124*, 164707.
(32) Venables, J. A.; Spiller, G. D. T.; Hanbücken, *Rep. Prog. Phys.* **1984**, *47*, 399.
(33) Pai, W. W.; Hsu, C.-L.; Lin, M. C.; Lin, K. C.; Tang, T. B. *Phys. Rev. B* **2004**, *69*, 125405.
(34) Muntwiler, M.; Auwärter, W.; Seitsonen, A. P.; Osterwalder, J.; Greber, T. *Phys. Rev. B* **2005**, *71*, 121402.
(35) Schwedhelm, R.; Schlomka, J.-P.; Woedtke, S.; Adelung, R.; Kipp, L.; Tolan, M.; Press, W.; Skibowski, M. *Phys. Rev. B* **1999**, *59*, 13394.
(36) Reinke, P.; Feldemann, H.; Oelhafen, P. *J. Chem. Phys.* **2003**, *119*, 12547.
(37) Burke, S. A.; Mativetsky, J. M.; Hoffmann, R.; Grütter, P. *Phys. Rev. Lett.* **2005**, *94*, 096102.
(38) Pai, W. W.; Hsu, C.-L.; Chiang, C. R.; Chang, Y.; Lin, K. C. *Surf. Sci.* **2002**, *519*, L605.
(39) Hsu, C.-L.; Pai, W. W. *Phys. Rev. B* **2003**, *68*, 245414.
(40) Pai, W. W.; Hsu, C.-L. *Phys. Rev. B* **2003**, *68*, 121403.
(41) Murray, P. W.; Pedersen, M. O.; Lægsgaard, E.; Stensgaard, I.; Besenbacher, F. *Phys. Rev. B* **1997**, *55*, 9360.